fields. They also indicate that the SCR theory does work in temperatures extremely close to the transition temperature.

To our knowledge, this is the first experimental work to show the divergent behavior of $1/T_1$ at $T_c$ in weak itinerant-electron ferromagnetic systems, and we conclude that there is general agreement between the present experimental results and the SCR theory. We would also like to mention that the capabilities and usefulness of a new technique, muon-spin rotation especially the longitudinal-field method, have been fully demonstrated here, in a current problem of magnetism study inaccessible to conventional NMR techniques.

The authors would like to thank Dr. J. T. Sample and the TRIUMF staff for their hospitality and encouragement. We would also like to thank Dr. J. H. Brewer, Dr. K. Nagamine, Professor R. Kubo, and Professor T. Moriya for helpful discussions and encouragement. This work was supported by the Japan Society for the Promotion of Science, the Toray Science Foundation, the Grant-in-Aid of the Japanese Ministry of Education, Culture, and Science, and the Atomic Energy Control Board and National Research Council of Canada.

[1]K. Motoya, H. Yasuoka, Y. Nakamura, V. Jaccarino, and J. H. Wernick, J. Phys. Soc. Jpn. 44, 833 (1978).
[2]H. Yasuoka, V. Jaccarino, R. C. Sherwood, and J. H. Wernick, J. Phys. Soc. Jpn. 44, 842 (1978).
[3]Y. Ishikawa, K. Tajima, D. Bloch, and M. Roth, Solid State Commun. 19, 525 (1976); Y. Ishikawa, G. Shirane, J. A. Tarvin, and M. Kohgi, Phys. Rev. B 16, 4956 (1977).
[4]T. Moriya and A. Kawabata, J. Phys. Soc. Jpn. 34, 639 (1973); T. Moriya and K. Ueda, Solid State Commun. 15, 169 (1974); T. Moriya, Physica (Ultrecht) 86-88B, 356 (1977).
[5]K. Makoshi and T. Moriya, J. Phys. Soc. Jpn. 44, 80 (1978).
[6]H. Yasuoka, R. S. Hayano, N. Nishida, K. Nagamine, and T. Yamazaki, Solid State Commun. 26, 745 (1978).
[7]R. S. Hayano, Y. J. Uemura, J. Imazato, N. Nishida, K. Nagamine, T. Yamazaki, and H. Yasuoka, Phys. Rev. Lett. 41, 421 (1978).
[8]R. Kubo and T. Toyabe, *Magnetic Resonance and Relaxation*, edited by R. Blinc (North-Holland, Amsterdam, 1967), p. 810.
[9]R. S. Hayano, Y. J. Uemura, J. Imazato, N. Nishida, and T. Yamazaki, to be published.

## Role of Local Plasmon Modes in Light Emission from Small-Particle Tunnel Junctions

R. W. Rendell and D. J. Scalapino
*Department of Physics, University of California, Santa Barbara, California 93106*

and

B. Mühlschlegel
*Institut für Theoretische Physik, Universität zu Köln, 5000 Köln 41, Germany*
(Received 2 October 1978)

A resonancelike structure has been reported in the frequency spectrum of light emitted from small-particle tunnel junctions. Here we present a calculation of the frequency-dependent dipole moment and the radiation emission spectrum for a small particle located above a metal film. The dipole moment exhibits a resonance structure associated with a localized surface plasma mode at a frequency corresponding to the peak in the structure observed in the emission spectra.

Small metal particles deposited on an oxidized metal film emit light when driven by inelastic tunneling electrons. In this process, the particle-film system acts as an antenna and the inelastic tunneling electrons as a current generator. In a previous analysis, the induced dipole moment of the antenna was calculated within a quasistatic limit appropriate for frequencies well below the plasma resonance threshold.[1] Experimental studies of the intensity spectra from tunnel junctions formed by depositing gold particles onto an oxidized aluminum film exhibit a resonancelike structure near 650 nm (1.9 eV).[2] Here we report calculations which suggest that this structure arises from local plasma resonant modes of the gold-particle–aluminum-film system.

Figure 1 shows the geometry of the small-par-

 

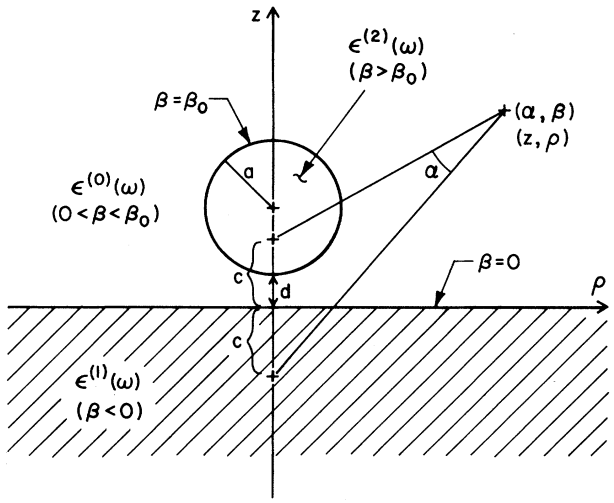


FIG. 1. The geometry of the small-particle–film system using bispherical coordinates $(\alpha,\beta)$.

ticle–film system. A typical particle radius $a$ is of order 100–200 Å, while the particle-film separation $d$ is about one-tenth of this. Since the particle size is small compared to the wavelength of light, we can neglect retardation. Furthermore, the tunneling charge transfer is localized near the region of closest contact between the particle and the film so that it can be well approximated by a local source.

Before discussing the details of the calculation, it is useful to make some physical estimates. If the gold particles were replaced by a gold film, the Au-$Al_2O_3$-Al interface would support an interface plasma resonance. For thick films, neglecting retardation, the dispersion relation for this mode with wave vector $q$ is known to vary as $\bar{\omega}_p(qd)^{1/2}\epsilon_0^{-1/2}$ at long wavelengths.[3] Here $\bar{\omega}_p$ is the reduced average plasma frequency of the two metals, and $\epsilon_0$ is the dielectric constant of the oxide. Now, in the case of a small particle, the translational invariance is broken, and these surface plasma modes become localized under the particle. A simple estimate, based on the length over which there is a doubling of the particle-film spacing, shows that the mode is localized over a distance set by the geometric mean of the particle radius and the particle-film separation distance, $(ad)^{1/2}$. The frequency of a surface plasma mode with $q\sim(ad)^{-1/2}$ is of order $\bar{\omega}_p(d/a)^{1/4}\epsilon_0^{-1/2}$. Within a numerical factor of order 1, this is just what we find for the lowest mode of the particle-film system in the calculations outlined below. Lying above this are an infinite, discrete set of levels which cut off at the upper frequency limit of the Au surface plasmon. Damping broadens these modes so that they overlap, and the interband transitions in Au damp the higher-frequency ones. In the calculations leading to Figs. 2 and 3, the imaginary parts of the dielectric constants for Au and Al have been included. In addition, the dipole form factor emphasizes the lower modes. The resulting dipole moment shown in Fig. 2 reflects these features, exhibiting a maxima near $\bar{\omega}_p(d/a)^{1/4}\epsilon_0^{-1/2}$.

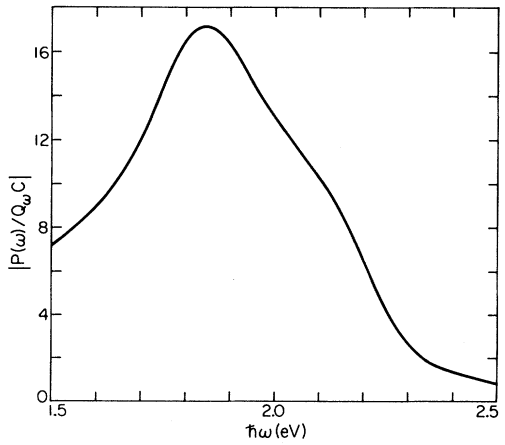


FIG. 2. The calculated dipole moment in the resonance region of a gold-sphere–aluminum-film system. Here $\epsilon^{(1)}$ and $\epsilon^{(2)}$, the complex frequency-dependent dielectric constants for Al and Au, respectively, were taken from experimental optical data (Ref. 5) and the values $\beta_0\simeq(2d/a)^{1/2}=0.3$ and $\epsilon^{(0)}=3$ were used.

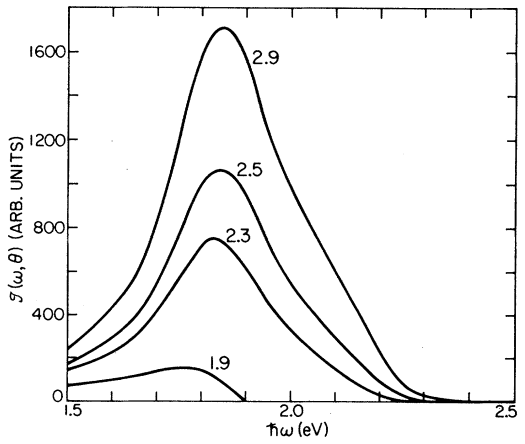


FIG. 3. The calculated emission spectrum from the gold-sphere–aluminum-film tunnel junction for several bias voltages. The values $\beta_0\simeq(2d/a)^{1/2}=0.3$, $\epsilon^{(0)}=3$, and $\theta=60°$ were used.

In order to calculate the dipole moment, we must solve first for the potential $\varphi$ determined by

$$\nabla\cdot[\epsilon(\vec{x},\omega)\nabla\varphi]=-4\pi\rho_\omega(\vec{x}). \quad (1)$$

Here $\epsilon(\vec{x},\omega)$ takes on the value $\epsilon^{(1)}(\omega)$ in the film, $\epsilon^{(0)}(\omega)$ in the oxide, and $\epsilon^{(2)}(\omega)$ in the particle. On a scale of distance $(ad)^{1/2}$, the charge transfer associated with inelastic electron tunneling is well approximated by the local form

$$\rho_\omega=Q_\omega[\delta(z-d)-\delta(z)]\delta(\rho)/2\pi\rho. \quad (2)$$

As discussed in Ref. 1, $|Q_\omega|^2=|i_\omega/\omega|^2$ with $|i_\omega|^2=(eV/2\pi R)(1-\hbar\omega/eV)$, the inelastic tunneling-current power spectrum. In this expression $V$ is the junction bias voltage, and $R$ is the tunneling resistance between the particle and the film.

It is convenient to make use of bispherical coordinates,[4] shown in Fig. 1, in which

$$\rho=\frac{c\sin\alpha}{\cosh\beta-\cos\alpha}, \quad z=\frac{c\sin\beta}{\cosh\beta-\cos\alpha}, \quad (3)$$

where $c=(d^2+2ad)^{1/2}$. After extracting a factor $[2(\cosh\beta-\cos\alpha)]^{1/2}$, Laplace's equation separates, and for the case of cylindrical symmetry the potential $\varphi$ can be written in the form

$$\varphi^{(i)}(\alpha,\beta)=[2(\cosh\beta-\cos\alpha)]^{1/2}\sum_{n=0}^{\infty}\{A_n^{(i)}\exp[-(n+\tfrac{1}{2})(\beta-\beta_0)]+B_n^{(i)}\exp[(n+\tfrac{1}{2})(\beta-\beta_0)]\}P_n(\cos\alpha). \quad (4)$$

Here the coefficients $A_n^{(i)}$ and $B_n^{(i)}$ take on different values in the three different regions corresponding to $i=1$, in the metal film ($\beta<0$); $i=0$, between the particle and the metal film ($0<\beta<\beta_0$); and $i=2$, inside the particle ($\beta_0<\beta$). In the first region, $A_n^{(1)}$ vanishes, while in the third region $B_n^{(2)}$ must vanish. Since the particle size $a$ is small compared to the wavelength of light, the intensity of the emitted radiation is determined by the dipole part $P$ of $\varphi$. Making a multipole expansion of $\varphi$ in bispherical coordinates, we obtain

$$P(\omega)=(2c)^2\sum_{n=0}^{\infty}(n+\tfrac{1}{2})\{-A_n^{(0)}\exp[(n+\tfrac{1}{2})\beta_0]+B_n^{(0)}\exp[-(n+\tfrac{1}{2})\beta_0]\}. \quad (5)$$

Applying the usual boundary conditions in which the tangential component of $\vec{E}$ is continuous and the discontinuity in the normal component of $\vec{D}$ is equal to $4\pi$ times the surface charge at the interfaces gives an infinite set of coupled linear equations relating the various $A_n^{(i)}$ and $B_n^{(i)}$ coefficients. For purposes of extracting the induced dipole moment it is convenient to relate all coefficients to $A_n^{(0)}$ and $B_n^{(0)}$ which satisfy the equations

$$A_n^{(0)}=\Gamma_n+\chi^{(1)}\exp[-(2n+1)\beta_0]B_n^{(0)} \quad (6)$$

and

$$\frac{\epsilon^{(0)}+\epsilon^{(2)}}{2c}\{[\sinh\beta_0\bar{\chi}_n+(2n+1)\cosh\beta_0](\bar{B}_n-\chi^{(2)}\Gamma_n)-(n+1)(\bar{B}_{n+1}-\chi^{(2)}\Gamma_{n+1})-n(\bar{B}_{n-1}-\chi^{(2)}\Gamma_{n-1})\}$$

$$=4\pi S_n-\frac{\epsilon^{(0)}+\epsilon^{(2)}}{2c}\Gamma_n\sin\beta_0\chi^{(2)}(1+\chi^{(2)})\{1-\chi^{(2)}\chi^{(1)}\exp[-(2n+1)\beta_0]\}^{-1}, \quad (7)$$

with

$$\bar{B}_n=\{1-\chi^{(2)}\chi^{(1)}\exp[-(2n+1)\beta_0]\}B_n^{(0)}, \quad \bar{\chi}_n=\chi^{(2)}\frac{1+\chi^{(1)}\exp[-(2n+1)\beta_0]}{1-\chi^{(2)}\chi^{(1)}\exp[-(2n+1)\beta_0]},$$

$$\chi^{(i)}=\frac{\epsilon^{(0)}-\epsilon^{(i)}}{\epsilon^{(0)}+\epsilon^{(i)}}, \quad \Gamma_n=\frac{-2(Q_\omega/c)(-1)^n}{\epsilon^{(0)}+\epsilon^{(i)}}\exp[-(n+\tfrac{1}{2})\beta_0], \quad S_n=(2n+1)\frac{Q_\omega/c^2}{2\pi}(-1)^n\left[\frac{\cosh\beta_0+1}{2}\right]^{3/2}. \quad (8)$$

The results for $P(\omega)$ shown in Fig. 2 were obtained by truncating the set of linear equations (6)–(8) and numerically solving for the coefficients. Experimental data were used for the complex dielectric constants $\epsilon^{(1)}(\omega)$ and $\epsilon^{(2)}(\omega)$ for Al and Au, respectively.[5] The results converged rapidly when more than fifteen terms were included.

Although we have not obtained a general analytic solution of the coupled equations, we have solved the case of an ideal particle ($\omega_p^{(2)}\gg\omega$ so that $\epsilon^{(2)}\to-\infty$) above an arbitrary film. In this case, we find

$$P(\omega)=2\epsilon^{(1)}\sum_{n=0}^{\infty}(2n+1)\exp[-(n+\tfrac{1}{2})\beta_0]\left[\frac{(-1)^nQ_\omega c}{\epsilon^{(0)}+\epsilon^{(1)}}+\varphi(\beta_0)c^2\right][\epsilon^{(0)}\cosh(n+\tfrac{1}{2})\beta_0+\epsilon^{(1)}\sinh(n+\tfrac{1}{2})\beta_0]^{-1} \quad (9)$$

with $\varphi(\beta_0)$ the equipotential on the sphere,

$$\varphi(\beta_0)=\frac{Q_\omega/c}{\epsilon^{(0)}(\epsilon^{(0)}+\epsilon^{(1)})}\frac{\frac{1}{2}-\sum_{n=0}^{\infty}\frac{(-1)^n\epsilon^{(0)}\exp[-(n+\frac{1}{2})\beta_0]}{\epsilon^{(0)}\cosh(n+\frac{1}{2})\beta_0+\epsilon^{(1)}\sinh(n+\frac{1}{2})\beta_0}}{\sum_{n=0}^{\infty}\frac{\exp[-(n+\frac{1}{2})\beta_0]}{\epsilon^{(0)}\cosh(n+\frac{1}{2})\beta_0+\epsilon^{(1)}\sinh(n+\frac{1}{2})\beta_0}}. \tag{10}$$

The interpretation of this form for $P(\omega)$ is simple. The denominators vanish at a set of discrete resonant modes of the sphere-plane system determined by

$$\tanh(n+\tfrac{1}{2})\beta_0=-\epsilon^{(0)}(\omega)/\epsilon^{(1)}(\omega). \tag{11}$$

For a free-electron metal film with $\epsilon^{(1)}(\omega)=1-(\omega_p/\omega)^2$ and constant $\epsilon^{(0)}$, these resonant frequencies occur at

$$\omega_n=\omega_p\left(\frac{\tanh(n+\frac{1}{2})\beta_0}{\epsilon^{(0)}+\tanh(n+\frac{1}{2})\beta_0}\right)^{1/2}. \tag{12}$$

Since $\beta_0=\cosh^{-1}(1+d/a)\cong(2d/a)^{1/2}$, the lowest mode $\omega_0$ is approximately equal to $\omega_p/(\epsilon^{(0)})^{1/2}(d/2a)^{1/4}$, and the upper cutoff for $n\to\infty$ is just $\omega_p[\epsilon^{(0)}+1]^{-1/2}$. The variation of $\omega_0$ with particle size and oxide thickness should be tested experimentally. As discussed above, the lowest mode corresponds to a surface plasmon localized in a region of order $(ad)^{1/2}$. As $n$ increases, the modes approach the limit appropriate to the short-wavelength surface plasma frequency of the $\epsilon^{(1)}(\omega)$-$\epsilon^{(0)}$ interface. The form factor in the numerator of Eq. (9) contains a factor $\exp[-(n+\frac{1}{2})\beta_0]$ which suppresses the higher-order modes reflecting the fact that they have less dipole character. As noted, these analytic results do not include the absorptive part of $\epsilon$. This was, however, included in the numerical results shown in Figs. 2 and 3. It is interesting to note that the zero-frequency limit of Eq. (9) gives the static case investigated in Ref. 1:

$$\begin{aligned}\varphi(\beta_0)&\simeq\frac{Q_\omega/c}{2\epsilon^{(0)}}\left(\sum_{n=0}^{\infty}\frac{2}{\exp[(2n+1)\beta_0]-1}\right)^{-1}\to\frac{Q_\omega/c}{8\epsilon^{(0)}}\frac{2\beta_0}{\ln(1/\beta_0)},\\ P(0)&\simeq 4\varphi(\beta_0)c^2\sum_{n=0}^{\infty}\frac{2n+1}{\exp[(2n+1)\beta_0]-1}\simeq\frac{4\varphi(\beta_0)c^2}{\beta_0^2}\frac{\pi^2}{12}\to\frac{2}{3}\pi^2\frac{Q_\omega c}{2\beta_0\epsilon^{(0)}\ln(1/\beta_0)}.\end{aligned} \tag{13}$$

The power radiated per unit solid angle $\Delta\Omega$ and per unit frequency $\Delta\omega$ is given by

$$g(\theta,\omega)\Delta\omega\Delta\Omega=\frac{|P(\omega)|^2\omega^4}{8\pi c^3}\sin^2\theta|1+\Gamma(\omega,\theta)|^2\Delta\omega\Delta\Omega,$$

with

$$\Gamma(\omega,\theta)=\frac{(\epsilon^{(1)}/\epsilon^{(0)})^{1/2}\cos\theta-[1-(\epsilon^{(0)}/\epsilon^{(1)})\sin^2\theta]^{1/2}}{(\epsilon^{(1)}/\epsilon^{(0)})^{1/2}\cos\theta+[1-(\epsilon^{(0)}/\epsilon^{(1)})\sin^2\theta]^{1/2}}.$$

The factor $\Gamma$ takes into account the effect of the Al film on the dipole emission. For radiation in the visible, it gives rise to a peak in the angular distribution at $\theta\simeq 60°$ from the normal in agreement with the data of Ref. 2. Using the full expression for $P(\omega)$ given by Eq. (5) we show the shape of $g(\theta,\omega)$ in Fig. 3 for $\theta=60°$ and various bias voltages. The effect of the plasmon resonance is to produce a peak in $g(\theta,\omega)$ whose position is independent of the bias voltage. Furthermore, beyond the peak the intensity rapidly drops off. The experimental data of Ref. 2 shows a definite peak near 1.9 eV and a rapid decrease of the intensity above this. However, the experimental data do not drop as rapidly as the theoretical results at lower frequencies. We believe that this is associated with particle clumping which effectively increases the size of the region over which the plasma excitation is localized and lowers the resonance frequency. The distribution of single particles, pairs, and larger clumps would produce a smearing below the single-particle resonance peak. Experiments are in progress to study dilute, separate-particle junctions.

The authors would like to acknowledge many helpful discussions with their colleagues H. Broida, P. Hansma, and D. Hone. This work was supported by the National Science Foundation.

[1]D. Hone, B. Mühlschlegel, and D. J. Scalapino, Appl.

Phys. Lett. 33, 203 (1978).
[2]P. K. Hansma and H. P. Broida, Appl. Phys. Lett. 32, 545 (1978).
[3]H. Raether, Phys. Thin Films 9, 145 (1977).
[4]P. M. Morse and H. Feshbach, *Methods of Theoretical Physics* (McGraw-Hill, New York, 1953), Vol. I, p. 665.
[5]H.-J. Hagemann, W. Gudat, and C. Kunz, J. Opt. Soc. Am. 65, 742 (1975), and DESY Report SR-74/7, (unpublished).

# Band-Gap Assignment in $SnO_2$ by Two-Photon Spectroscopy

D. Fröhlich and R. Kenklies
*Institut für Physik, Universität Dortmund, 46 Dortmund, Federal Republic of Germany*

and

R. Helbig
*Institut für Angewandte Physik, Universität Erlangen-Nürnberg, 852 Erlangen, Federal Republic of Germany*

(Received 2 October 1978)

We present for the first time two-photon measurements on rutile $SnO_2$. The detailed polarization analysis yields $\Gamma_3^+$ symmetry for the direct forbidden 1*S* exciton and the upper valence band. Our results clear up the long-standing controversy concerning the symmetry of the upper valence band.

As proposed by Loudon,[1] the direct forbidden transitions are specially suited to be studied by two-photon spectroscopy. Loudon calculated the two-photon absorption for $Cu_2O$, which was later studied by Pradère and co-workers.[2] Because of experimental difficulties these authors found only a weak structure, which they attribute to the 1*S* exciton. They were not able to measure the polarization dependence. We present for the first time a detailed polarization analysis of such a direct forbidden transition. Using this technique we are able to resolve the long-standing puzzle on the band-gap assignment in $SnO_2$ ($D_{4h}^{14}$).

Though the early indication of $SnO_2$ being an indirect material[3,4] could no longer be maintained after the excellent work of Nagasawa and Shionoya,[5] the symmetry assignment of the direct gap remained as a controversy. Nagasawa and Shionoya were able to show that the band gap is direct forbidden at $\vec{K} = 0$. They offer three possibilities for the highest valence band ($\Gamma_2^+, \Gamma_3^+, \Gamma_4^+$) assuming a $\Gamma_1^+$ lowest conduction band, which is agreed on in later experimental[6,7] as well as theoretical investigations.[8,9] Agekyan[10] analyzed the quadrupole transition to the 1*S* exciton and determined $\Gamma_3^+$ symmetry for the top valence band. There are two band-structure calculations[8,9] published which contradict each other as well as the assignment of Agekyan. Arlinghaus[8] assigns the top valence band to be of $\Gamma_1^+$ symmetry whereas Jacquemin[9] comes up with a $\Gamma_5^+$ valence band. Jacquemin states that his assignment is compatible with the experimental results of Agekyan.[10] A third band-structure calculation was very recently presented by Robertson,[11] who calculated the highest valence band to be of $\Gamma_3^+$ symmetry. In order to clear up this controversy, we present two-photon data on the lowest exciton. A complete polarization analysis of this transition allows an unambiguous assignment of the upper valence band to $\Gamma_3^+$ symmetry.

Our basic experimental setup is described in detail by Fröhlich and Sondergeld.[12] To improve

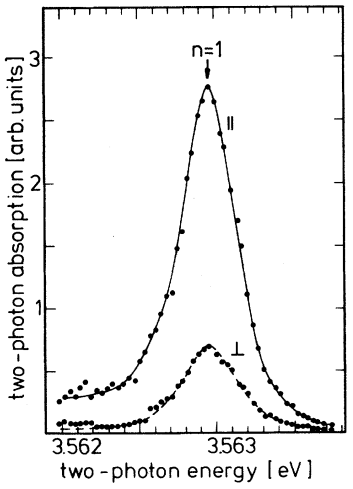


FIG. 1. Two-photon spectra of 1*S* exciton in rutile $SnO_2$ at 4.5 K (resolution 0.15 meV). ∥ configuration (0°/0°), both polarization vectors $\vec{\epsilon}_1$ and $\vec{\epsilon}_2$ parallel to [100]; ⊥ configuration (0°/90°), $\vec{\epsilon}_1$ in [100] and $\vec{\epsilon}_2$ in [010] directions.